# Distribution and dynamics of Lamp1-containing endocytic organelles in fibroblasts deficient in BLOC-3

**Juan M. Falcón-Pérez, Ramin Nazarian, Chiara Sabatti and Esteban C. Dell'Angelica***

Department of Human Genetics, University of California, Los Angeles, CA 90095, USA

*Author for correspondence (e-mail: edellangelica@mednet.ucla.edu)

*Accepted 12 August 2005*
*Journal of Cell Science 118, 5243-5255 Published by The Company of Biologists 2005*
*doi:10.1242/jcs.02633*

## Summary

**Late endosomes and lysosomes of mammalian cells in interphase tend to concentrate in the perinuclear region that harbors the microtubule-organizing center. We have previously reported abnormal distribution of these organelles – as judged by reduced percentages of cells displaying pronounced perinuclear accumulation – in mutant fibroblasts lacking BLOC-3 (for 'biogenesis of lysosome-related organelles complex 3'). BLOC-3 is a protein complex that contains the products of the genes mutated in Hermansky-Pudlak syndrome types 1 and 4. Here, we developed a method based on image analysis to estimate the extent of organelle clustering in the perinuclear region of cultured cells. Using this method, we corroborated that the perinuclear clustering of late endocytic organelles containing Lamp1 (for 'lysosome-associated membrane protein 1') is reduced in BLOC-3-deficient murine fibroblasts, and found that it is apparently normal in fibroblasts deficient in BLOC-1 or BLOC-2, which are another two protein complexes associated with Hermansky-Pudlak syndrome. Wild-type and mutant fibroblasts were transfected to express human LAMP1 fused at its cytoplasmic tail to green fluorescence protein (GFP). At low expression levels, LAMP1-GFP was targeted correctly to late endocytic organelles in both wild-type and mutant cells. High levels of LAMP1-GFP overexpression elicited aberrant aggregation of late endocytic organelles, a phenomenon that probably involved formation of anti-parallel dimers of LAMP1-GFP as it was not observed in cells expressing comparable levels of a non-dimerizing mutant variant, LAMP1-mGFP. To test whether BLOC-3 plays a role in the movement of late endocytic organelles, time-lapse fluorescence microscopy experiments were performed using live cells expressing low levels of LAMP1-GFP or LAMP1-mGFP. Although active movement of late endocytic organelles was observed in both wild-type and mutant fibroblasts, quantitative analyses revealed a relatively lower frequency of microtubule-dependent movement events, either towards or away from the perinuclear region, within BLOC-3-deficient cells. By contrast, neither the duration nor the speed of these microtubule-dependent events seemed to be affected by the lack of BLOC-3 function. These results suggest that BLOC-3 function is required, directly or indirectly, for optimal attachment of late endocytic organelles to microtubule-dependent motors.**

Key words: Lysosomes, Endosomes, Microtubules, Time-lapse microscopy, Hermansky-Pudlak syndrome

## Introduction

Organelles of the endocytic pathway undergo active movement mediated by microtubule- or actin-dependent motors, and display characteristic intracellular distributions in most mammalian cells during interphase (reviewed by Schroer, 2000). For instance, early endosomes containing the protein marker EEA1 (for 'early endosome antigen 1') tend to distribute more peripherally than late endocytic organelles (late endosomes and lysosomes) containing Lamp1 (for 'lysosome-associated membrane protein 1'), which normally accumulate in a juxtanuclear region around the microtubule-organizing center (MTOC) (Matteoni and Kreiss, 1987; Mu et al., 1995; Patki et al., 1997). The physiological significance of the movement and steady-state localization of these organelles remains incompletely understood, although it might contribute to the overall efficacy of the processes of organelle biogenesis and protein sorting.

The perinuclear steady-state distribution of lysosomes has been shown to reflect a balance between long-range vectorial movement towards the plus and minus ends of microtubules as well as short-range movement on actin filaments (Matteoni and Kreiss, 1987; Taunton et al., 2000; Cordonnier et al., 2001). Molecular motors implicated in the movement of lysosomes (and probably of late endosomes) include dynein and its associated dynactin complex (for movement towards the minus end of microtubules), kinesin superfamily members such as KIF2β and KIF1Bβ3 (for microtubule-dependent movement towards the cell periphery) and myosin Iα (for movement on actin filaments) (Burkhardt et al., 1997; Harada et al., 1998; Santama et al., 1998; Valetti et al., 1999; Cordonnier et al., 2001; Matsushita et al., 2004). Other factors include: Rab7 and its effector, Rab7-interacting lysosomal protein, which regulate attachment of late endocytic organelles to dynactin/dynein (Jordens et al., 2001); and MLN64, which regulates attachment

of these organelles to actin filaments (Hölttä-Vuori et al., 2005). Interference with the function of these proteins, either by loss-of-function or overexpression approaches, has been reported to modify the steady-state distribution of late endosomes and lysosomes, as inferred from fluorescence microscopic analyses (Burkhardt et al., 1997; Harada et al., 1998; Santama et al., 1998; Valetti et al., 1999; Bucci et al., 2000; Cantalupo et al., 2001; Cordonnier et al., 2001; Matsushita et al., 2004; Hölttä-Vuori et al., 2005).

We (Nazarian et al., 2003) and others (Chiang et al., 2003; Martina et al., 2003) have described a stable protein complex, named BLOC-3 (for 'biogenesis of lysosome-related organelles complex 3), which is expressed ubiquitously and contains the products of the *HPS1* and *HPS4* genes mutated in Hermansky-Pudlak syndrome (HPS) types 1 and 4, respectively. HPS is a group of autosomal recessive disorders involving defects in lysosome-related organelles (reviewed by Di Pietro and Dell'Angelica, 2005). Common to all forms of HPS are albinism and bleeding diathesis, resulting from abnormalities in melanosomes and platelet dense granules, respectively. Patients suffering from HPS-1 and HPS-4 are at risk of developing progressive pulmonary fibrosis, which might arise from defects in another lysosome-related organelle, the lamellar body of type II lung epithelial cells. A mild form of ceroid lipofuscinosis has also been described for HPS type 1 patients, suggesting that lysosomal degradative function might be compromised (reviewed by Gunay-Aygun et al., 2004). The murine orthologs of human *HPS1* and *HPS4* are mutated in the pale ear and light ear strains, respectively, which serve as bona fide models of the disease (Li et al., 2004). Using immortalized fibroblasts derived from the skin of these mutant mice, we observed relatively reduced percentages of cells displaying pronounced perinuclear distribution at steady-state of markers of late endosomes (lysobisphosphatidic acid), lysosomes (internalized dextran), or both (Lamp1). Colocalization experiments indicated that the observed differences were unlikely to be owing to protein missorting, suggesting that BLOC-3 might regulate the movement/distribution of late endosomes and lysosomes (Nazarian et al., 2003).

In this work, we sought to develop a quantitative method to estimate the extent of organelle clustering at the perinuclear region of the cell, which has so far relied on intrinsically subjective approaches. We applied this method to the analysis of Lamp1-positive organelles in mutant fibroblasts deficient in BLOC-3 as well as in BLOC-1 or BLOC-2, another two protein complexes associated with HPS (Di Pietro and Dell'Angelica, 2005). We also performed time-lapse microscopic experiments on live cells expressing human LAMP1 fused to green fluorescence protein (GFP), to test the hypothesis that BLOC-3 plays a role in the regulation of the movement of late endocytic organelles. During the course of these experiments, we observed that high levels of LAMP1-GFP overexpression can elicit organelle aggregation, and examined the possible mechanism of this phenomenon.

## Materials and Methods

### Reagents

The sources of primary and secondary antibodies used in this study were described previously (Nazarian et al., 2003). Texas-Red- and BODIPY-FL-conjugated fixable dextrans were purchased from Molecular Probes. The human megakaryoblast cell line MEG-01 was obtained from American Type Culture Collection. All media and reagents for tissue culture, as well as the TRIzol reagent, were purchased from Invitrogen. The FuGENE 6 transfection reagent was from Roche Diagnostics. Nocodazole was from Sigma-Aldrich. All other reagents were of analytical grade.

### DNA constructs

To generate an expression plasmid encoding the LAMP1-GFP fusion protein, the complete open-reading frame of human LAMP1 (GenBank accession number XM_052636) and portions of the 5′ and 3′ untranslated regions were amplified by reverse-transcriptase PCR from total RNA purified from MEG-01 cells using the TRIzol reagent. The product was purified and used as template for nested PCR using primers designed to append an *Eco*RI site upstream of the Kozak sequence and to replace the translation termination site by a segment encoding the linker sequence GSTGSTGSTGA (single-letter amino acid code) followed by a *Sal*I site. The nested PCR product was gel purified and cloned in the *Eco*RI-*Sal*I sites of the pEGFP-N3 vector (BD Biosciences Clontech). A variant construct expressing LAMP1-mGFP, in which the leucine residue at position 221 of the GFP domain was replaced by lysine to avoid anti-parallel dimerization (Zacharias et al., 2002), was generated by site-directed mutagenesis using the QuickChange XL kit (Stratagene). Constructs were verified by DNA sequencing.

### Cell culture, transfection and dextran internalization

The generation and culture conditions of immortalized fibroblast lines derived from the skin of wild-type (C57BL/6J), pale ear (B6.C3Fe-*Hps1*$^{ep}$/J), pallid (B6.Cg-*Pldn*$^{pa}$/J) and cocoa (B6.B10-*Hps3*$^{coa}$/J) mice were described previously (Nazarian et al., 2003; Di Pietro et al., 2004). Transient transfection using FuGENE 6 and labeling of lysosomes through internalization of Texas-Red-conjugated dextran were performed as described (Nazarian et al., 2003).

For stable transfection, murine fibroblasts were grown at 37°C in complete DMEM [Dulbecco's modified Eagle medium supplemented with 20% (v/v) fetal bovine serum, 2 mM glutamine, 0.1 mg/ml streptomycin and 100 units/ml penicillin] to 60-70% confluency, and subsequently transfected with the LAMP1-GFP-encoding plasmid using FuGENE 6 in serum-free DMEM. The medium was changed to complete DMEM 5 hours after transfection, and to complete DMEM containing 2 g/l G418 one day later. Cells displaying resistance to G418 and expressing LAMP1-GFP (as judged by fluorescence microscopy) were cloned by limiting dilution and, in the cases of one line derived from wild-type fibroblasts and one line derived from pale ear fibroblasts, by preparative cell sorting on a BD FACSVantage SE flow cytometer (Becton Dickinson).

### Fluorescence microscopy of fixed cells

Immunofluorescence staining of fixed/permeabilized cells was carried out as described (Dell'Angelica et al., 1997). The samples were examined on a Zeiss Axioskop 2 microscope equipped with an Orca-ER digital camera (Carl Zeiss) or, for analyses requiring high optical resolution (e.g. colocalization experiments), on a Leica TCS SP multiphoton confocal microscope (Leica).

### Determination of perinuclear clustering index

Fixed/permeabilized fibroblasts from wild-type, pallid, cocoa and pale ear mice (three independent cell lines per strain) were stained using rat monoclonal antibody 1D4B against endogenous murine Lamp1, followed by Cy3-conjugated secondary antibody against rat IgG. Digital images (1344×1024 pixels, 8 bits per pixel) of randomly selected cells were acquired on a Zeiss Axioskop 2

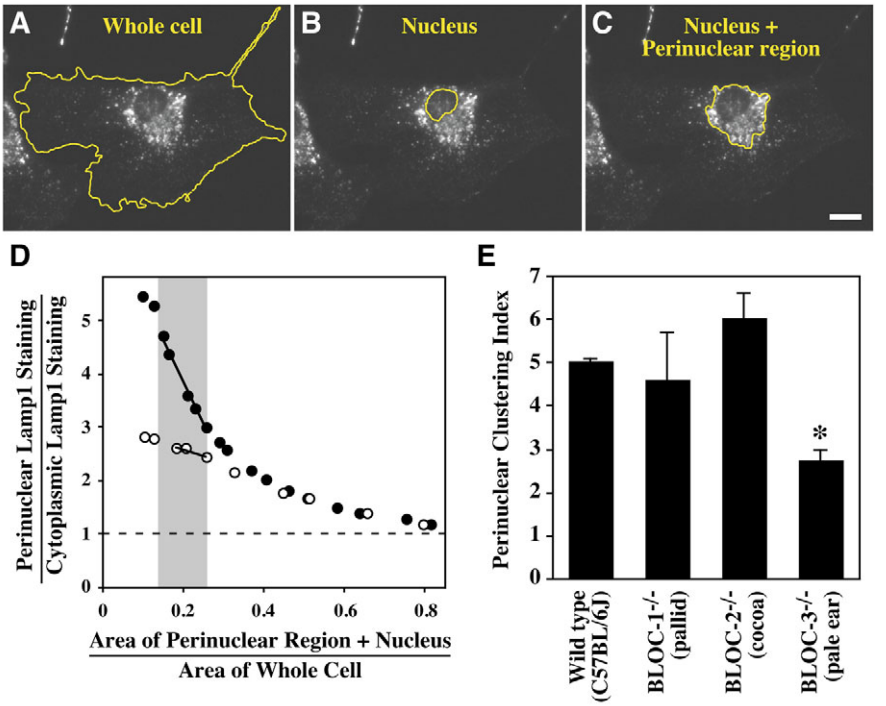


**Fig. 1.** Quantitative analysis of the perinuclear clustering of endogenous Lamp1 from wild-type and BLOC-deficient fibroblasts. (A-C) Low-magnification fluorescence images of cells stained with anti-Lamp1 were acquired using a fluorescence microscope equipped with a digital camera. Images were processed to calculate areas (in pixels) and mean fluorescence intensities (in arbitrary units) of (A) 'whole cell', (B) 'nucleus' and (C) 'nucleus + perinuclear region', which were drawn (yellow lines) by an operator who was unaware of the identity of the sample. Bar, 20 μm. (D) Plot of the ratio between background-corrected, mean fluorescence values of the regions defined as perinuclear (i.e. 'nucleus + perinuclear region' minus 'nucleus') and cytoplasmic (i.e. 'whole cell' minus 'nucleus') as a function of the ratio between the areas of 'nucleus + perinuclear region' and 'whole cell'. Filled circles correspond to values derived from the cell shown in A-C. Open circles correspond to the analysis of another cell in which Lamp1 staining was relatively less concentrated in the perinuclear area. For each cell, the perinuclear clustering index (PCI) was calculated as the slope obtained by linear regression of the data within the range of relative area sizes 0.15-0.25 (gray in D), multiplied by –1 to render positive values. (E) PCI of immortalized skin fibroblast lines derived from mutant murine strains deficient in BLOC-1 (pallid), BLOC-2 (cocoa) and BLOC-3 (pale ear), as well as from a wild-type control strain. For each cell line, the PCI of 20 randomly selected cells was averaged. Bars represent mean±standard error of three independent cell lines per strain. *$P$<0.05 (ANOVA followed by Tukey's test).

microscope equipped with an Orca-ER digital camera, using a 40× objective and appropriate filters. Two images were acquired for each selected microscopic field; one was obtained under conditions optimized to prevent signal saturation, and the other was overexposed to facilitate delimitation of the cell perimeter. The images were saved as TIFF files using coded file names, to ensure that the person(s) involved in subsequent image analysis could readily recognize which two files corresponded to the optimal and overexposed versions of each image but could not establish the identity of the cell line. Images were imported into NIH Image 1.62, using the Stacks option to align each pair of optimal and overexposed images. For each cell in the image, the perimeter of the whole cell (C) and that of the nucleus (N) were drawn by an operator (see, for example, Fig. 1A,B). Although drawing of these two perimeters was based on the overexposed version of the image, all calculations were performed using the optimal version. Additional areas, including the nucleus and part of the perinuclear region of the cell (nucleus + perinuclear, or NP), were delimited according to the following rules: (1) it must completely include the area delimited as the nucleus; (2) it must not extend outside the cell; and (3) its shape should maximize inclusion of Lamp1 staining signal (for example, see Fig. 1C). For each delimited region, its size (S, in pixels) and mean fluorescence intensity (F, in arbitrary units) were measured, and multiplication of these two values allowed calculation of the total fluorescence signal of the region. To calculate the uncorrected mean fluorescence intensity of the perinuclear (or cytoplasmic) regions, the total fluorescence signal of the N region was subtracted from that of the NP region (or of the C region), and the resulting value was divided by the size of NP (or of C) minus the size of N. A background mean fluorescence intensity, $F_B$, was measured from areas delimited at random places outside the cells and subtracted from the uncorrected mean fluorescence intensity values of the perinuclear and cytoplasmic regions. Hence, the perinuclear/cytoplasmic Lamp1 staining ratio (R) was calculated using the following equation:

$$R = [(F_{NP} \times S_{NP} - F_N \times S_N) / (S_{NP} - S_N) - F_B] / [(F_C \times S_C - F_N \times S_N) / (S_C - S_N) - F_B] . \quad (1)$$

Because the value of R was heavily dependent on the relative size of the NP area (Fig. 1D), a series of NP areas of increasing size were drawn for each cell, and those with relative area sizes ($S_{NP}/S_C$) in the 0.15-0.25 range (at least three data points per cell) were used for least-square fitting of the data by the following equation:

$$R = A - PCI \times (S_{NP} / S_C) , \quad (2)$$

where PCI (perinuclear clustering index) and A are the constants of the fitted linear equation.

### Time-lapse fluorescence microscopy

Fibroblasts were grown on glass-bottomed culture dishes (Mattek). Initial analyses of the dynamics of late endosomes and lysosomes were carried out using wild-type and mutant fibroblast lines stably expressing LAMP1-GFP, and subsequent experiments were performed using fibroblasts that had been transiently transfected to express LAMP1-GFP or LAMP1-mGFP. In all cases, cells expressing low levels of the fusion protein, as judged by GFP fluorescence, were selected for imaging. To prepare cell samples for the analysis of lysosome dynamics, cells were first incubated for 8 hours in complete DMEM containing 0.5 g/l BODIPY-FL-conjugated dextran, transferred to glass-bottomed culture dishes, and incubated for another 12 hours in complete DMEM lacking dextran, at 37°C in a tissue culture incubator.

For acquisition of time-lapse fluorescence images, the medium was changed to complete DMEM lacking Phenol Red and containing 25 mM Hepes buffer (pH 7.4), and the glass-bottomed culture dishes

were placed on the heating stage of a Leica DM-IRBE inverted microscope equipped with a 100× objective and Orca-ER digital camera, and controlled by SlideBook software (Intelligent Imaging Innovations, Denver, CO). The temperature of the sample was set to 35°C. In typical experiments, images were acquired every 2 seconds for 98 seconds, and pixel size was equivalent to 0.39×0.39 μm. In some experiments, cells were pre-incubated for at least 90 minutes in the presence of 30 μM nocodazole to disrupt microtubules.

For quantitative analysis of time-lapse experiments, 30 fluorescent organelles per cell were selected at random among those that were not in overcrowded regions of the initial frame image, and their positions determined in each subsequent frame by manual tracking. Because several organelles changed their shape during movement, their position was calculated as the center of mass of the fluorescence signal. The two-dimensional displacement between consecutive frames was calculated from the changes in X and Y position coordinates, using Pitagora's equation (changes in Z position were considered negligible due to the flat extended shape of the cells). For each organelle, the following values were calculated as defined: maximum speed (in μm/second) was defined as the highest value of speed (displacement divided by time) obtained between two consecutive frames; effective distance (in μm) was defined as the maximum distance between any two positions of the trajectory during the 98-second period; average speed on microtubules (in μm/second) was defined as the arithmetic average of all speed values between consecutive frames that were equal or larger than 0.78 μm/second; percentage of time at speed ≥0.78 μm/second was defined as the percentage of the 2-second intervals between frames in which the displacement was equal or larger than 1.56 μm; number of events with speed increasing to ≥0.78 μm/second was defined as the number of times within 98 seconds in which a 2-second interval with speed <0.78 μm/second was followed by another interval with speed ≥0.78 μm/second; and duration of events with speed ≥0.78 μm/second (in seconds) was defined as the arithmetic average of the duration of series of consecutive 2-second intervals with speed ≥0.78 μm/second.

### Statistical analyses

Statistical analysis of the PCI data was performed using one-way ANOVA followed by a posteriori Tukey's test, considering each average value per cell line (out of 20 randomly selected cells) an independent observation. For the analysis of data derived from time-lapse microscopic experiments, each median value per cell (out of 30 randomly selected organelles) was considered an independent observation. Ten cells were analyzed per cell line, and three (for LAMP1-GFP) or two (for LAMP1-mGFP) independent cell lines were analyzed per murine strain (wild-type or pale ear). The maximum speed, effective distance and average speed on microtubules data were analyzed using an ANOVA model upon logarithmic transformation (to make the assumption of Gaussian distributions appropriate). For the analysis of the percentage of time at speed ≥0.78 μm/second and the number of events with speed increasing to ≥0.78 μm/second data, the odds of obtaining zero as the median value per cell were compared using Fisher's exact test. The duration of events with speed ≥0.78 μm/second data was analyzed using both Kolmogorov-Smirnov test and Fisher's exact test.

## Results

### Quantitative analysis of perinuclear clustering

Previous analyses on the clustering of late endocytic organelles at the perinuclear region of the cell has relied on intrinsically subjective approaches, such as estimating percentages of cells that display pronounced perinuclear accumulation or perinuclear clustering as judged by an observer (e.g. Matteoni and Kreiss, 1987; Nazarian et al., 2003; Poupon et al., 2003; Matsushita et al., 2004; Gissen et al., 2005; Hölttä-Vuori et al., 2005). Although such approaches are simple and may suffice in cases where differences between cell samples are readily apparent, we sought to develop a quantitative method that would allow the study of perinuclear clustering in cases where differences may be relatively less dramatic.

We focused our analysis on late endosomes and lysosomes labeled with endogenously expressed Lamp1, which we previously reported to be relatively less concentrated in the perinuclear region of BLOC-3-deficient fibroblasts as inferred from reduced percentages of cells displaying pronounced perinuclear accumulation (Nazarian et al., 2003). Our approach consisted of estimating the concentration gradient of Lamp1 staining from determinations of the perinuclear/cytoplasmic staining ratio as a function of the relative size of the perinuclear region. We obtained digital images of Lamp1-stained cells under conditions in which the whole cell was included (i.e. low magnification and no optical sectioning) and the fluorescence signal intensities were within the dynamic range of the digital camera. To avoid bias in our analysis, the cells were randomly picked for imaging, and the resulting images were processed following a 'blinded' approach in which the operator was unaware of the sample identity.

Our attempts to develop an algorithm for fully automatic analysis of the images were hampered by the high variability in size and shape, not only of whole cells but also of their perinuclear regions. As an alternative, we chose to have an operator delimiting by hand (with the aid of a computer mouse) the whole cell (Fig. 1A), the nucleus (Fig. 1B) and a third area including the nucleus and part of the perinuclear region (Fig. 1C). Whereas definition of the first two regions was straightforward, the third was more problematic because we could not fit satisfactorily any simple geometrical shape to the NP region of most cells. Instead, the operator was allowed to delimit areas of any shape, with the main restriction that inclusion of Lamp1 staining should be maximized (e.g. see Fig. 1C). From each area we measured its size and mean fluorescence intensity, and using Equation 1 we calculated the perinuclear/cytoplasmic ratio of Lamp1 staining. As expected, this value was highly dependent on the relative size of the NP region area and approached unity as the size of this area approached that of the whole cell (Fig. 1D). Similar calculations performed for several cells led us to restrict our analysis to relative area sizes in the 0.15-0.25 range, in which the relationship between perinuclear/cytoplasmic staining ratio and relative area size could be fitted reasonably by a linear function (Fig. 1D, gray area). We defined the perinuclear clustering index (PCI) as the slope of the fitted linear function, multiplied by –1 to render positive values. Importantly, we found that the role of the operator in deciding the shape of the NP region area was not a major source of error, as the operator-to-operator variability in the analysis of the same set of cells (11%) was lower than the cell-to-cell variability within a fibroblast line (76%).

Using this quantitative approach, we re-examined the effect of BLOC-3 deficiency on perinuclear clustering of Lamp1-positive organelles in murine skin fibroblasts (Nazarian et al., 2003) and extended our analysis to fibroblasts deficient in BLOC-1 or -2, which are another two protein complexes of unknown molecular function but implicated in the pathogenesis of HPS. We used immortalized lines of skin

fibroblasts derived from a wild-type strain and from the pallid, cocoa and pale ear strains deficient in BLOC-1, -2 and -3, respectively. We analyzed three independent cell lines (derived from different animals) per strain; for each cell line, we calculated the PCI as the average of the values obtained for 20 randomly selected cells. The results are shown in Fig. 1E. Consistent with our previous study (Nazarian et al., 2003), the PCI of Lamp1 staining was significantly reduced in cells deficient in BLOC-3. By contrast, the PCI was not significantly affected in cells deficient in BLOC-1 or -2. Hence, normal perinuclear clustering of Lamp1-positive organelles in fibroblasts requires BLOC-3 function but seems not to depend on BLOC-1 or -2.

### The LAMP1-GFP fusion protein localizes to late endocytic organelles at low expression levels but its overexpression causes abnormal organelle aggregation

To characterize further the effects of BLOC-3 deficiency on Lamp1-positive late endosomes and lysosomes, we expressed a construct consisting of the human ortholog of murine Lamp1, LAMP1, fused at its cytoplasmic carboxyl terminus to GFP. We chose to fuse GFP to human LAMP1, and not to the murine protein, because of the availability of a species-specific rat monoclonal antibody, 1D4B, which recognizes mouse Lamp1 and not human LAMP1 and thus allows detection of endogenous Lamp1 in cells expressing the LAMP1-GFP construct. Control experiments using human M1 fibroblasts transfected with the LAMP1-GFP-encoding plasmid corroborated that the monoclonal antibody does not significantly crossreact with LAMP1-GFP, even at the highest expression levels achieved in this study (not shown). Fusion of GFP at the carboxyl terminus of human LAMP1 did not interfere with its subcellular targeting, as judged by extensive colocalization between LAMP1-GFP and endogenous Lamp1 (Fig. 2A-C). As expected, the LAMP1-GFP fusion protein localized to most lysosomes labeled with internalized dextran, as well as to dextran-negative organelles that probably represented late endosomes (Fig. 2D-F). In agreement with a previous study using a GFP-tagged form of the avian Lamp1 homolog, lgp120 (Patterson and Lipincott-Schwartz, 2002), LAMP1-GFP was also targeted to pre-formed lysosomes, as inferred from its partial localization to lysosomes that had been loaded with dextran before transfection with the LAMP1-GFP-encoding plasmid (not shown). At low expression levels, LAMP1-GFP colocalized poorly with the early endosomal marker EEA1 (Fig. 2G-I). The degrees of colocalization of LAMP1-GFP with endogenous Lamp1 (Fig. 2J-L), dextran-loaded lysosomes (Fig. 2M-O) and

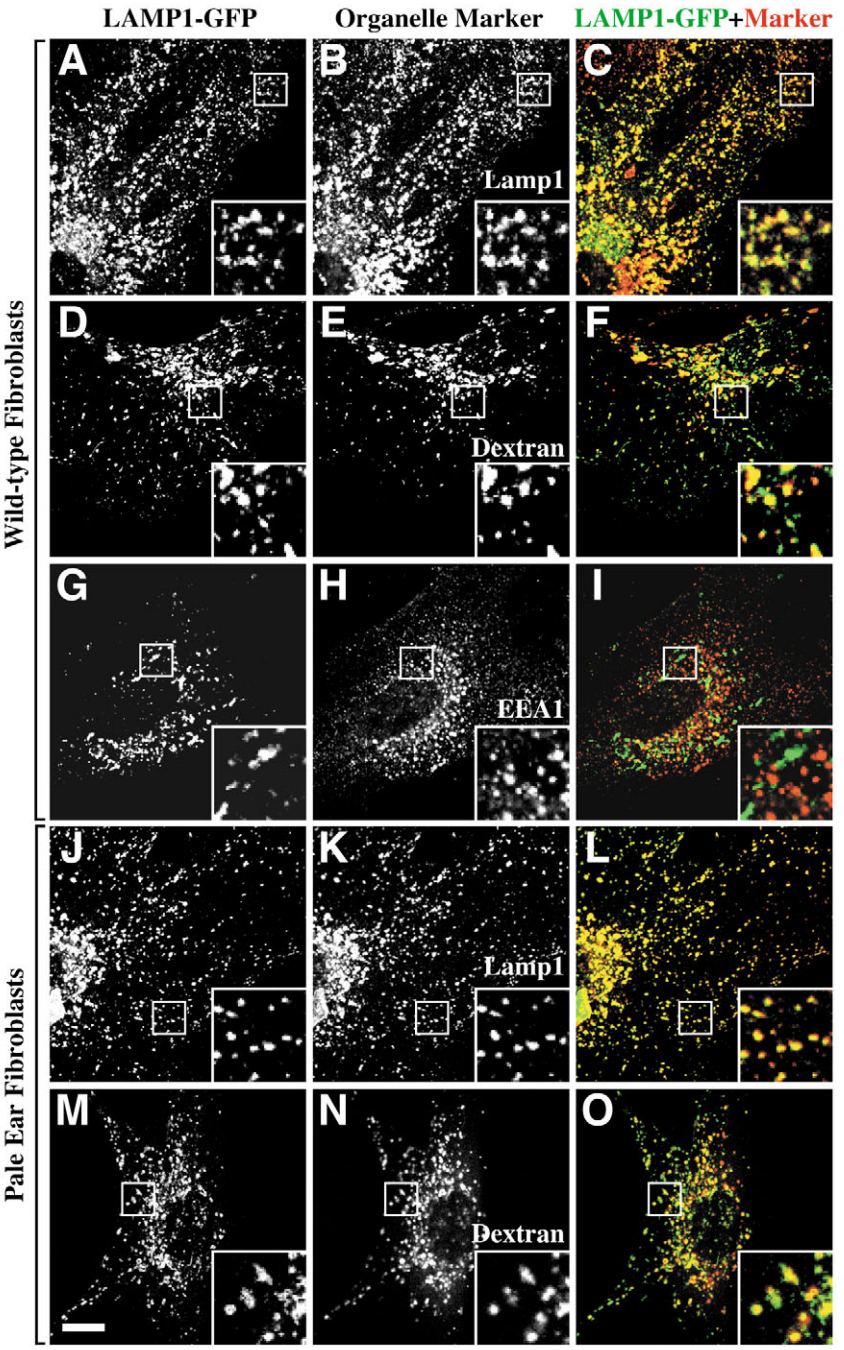


**Fig. 2.** Localization of LAMP1-GFP fusion protein expressed in transfected murine fibroblasts. Immortalized skin fibroblasts derived from wild-type (A-I) or pale ear (J-O) mice were transfected with a plasmid encoding human LAMP1 fused to GFP (A,D,G,J,M and green in C,F,I,L,O). One day after transfection, the cells were fixed/permeabilized and stained with a species-specific antibody to murine Lamp1 (B,K and red in C,L) or an antibody to EEA1 (H and red in I). Alternatively, cells were allowed to internalize Texas-Red-conjugated dextran, followed by a 4-hour chase period to ensure specific labeling of mature lysosomes (E,N and red in F,O). Bar, 20 μm. The top-left region of panels A-C, which displays staining of endogenous Lamp1 but not of LAMP1-GFP, corresponds to part of an untransfected cell. Magnified views of selected areas are shown in the insets.

EEA1 (not shown) in BLOC-3-deficient fibroblasts were similar to those observed in wild-type fibroblasts, implying that the steady-state localization of LAMP1-GFP was not significantly affected by BLOC-3 deficiency.

High levels of LAMP1-GFP overexpression not only led to accumulation of the chimeric protein at the cell surface and EEA1-positive compartments but, surprisingly, elicited aggregation of late endocytic compartments. Organelle aggregation in LAMP1-GFP-overexpressing cells was inferred from immunostaining of endogenous mouse Lamp1 (Fig. 3A-D) or labeling of lysosomes with fluorescent dextran either before (Fig. 3E,F) or after (not shown) transfection with the LAMP1-GFP-encoding plasmid. At low magnification, the staining appeared as 'chunky' (see Fig. 3B,D,F, arrows); however, close examination at high optical resolution by confocal microscopy revealed that the organelles were aggregated but not fused with each other (Fig. 3F, inset, and data not shown). A similar effect was observed upon expression of high levels of LAMP1-GFP in BLOC-3-deficient fibroblasts (Fig. 3I-L), indicating that BLOC-3 function is not required for this phenomenon. Further analyses (not shown) demonstrated that the same effect can be elicited upon overexpression of LAMP1-GFP in other cell lines (e.g. human HeLa and M1 cells) or by overexpression of another Lamp (LAMP3/CD63) tagged with GFP, and that early and recycling endosomes do not seem to be affected as judged by EEA1 and transferrin receptor immunostaining in LAMP1-GFP-overexpressing cells.

Previous studies have shown that microinjection of divalent antibodies to the cytoplasmic domain of LAMP1 can elicit aggregation of lysosomes (Bakker et al., 1997), and that overexpression of endoplasmic reticulum (ER)-resident membrane proteins fused to GFP at the cytoplasmic domain can induce stacked ER membrane structures resulting from low-affinity, anti-parallel dimerization of the GFP tag (Snapp et al., 2003). We hypothesized that the aberrant aggregation of late endosomes and lysosomes observed in cells expressing high levels of LAMP1-GFP could be owing to low-affinity binding of LAMP1-GFP from opposing membranes, through dimerization of their GFP tags. To test this hypothesis, we substituted leucine 221 of the GFP domain with lysine, a point mutation known to disrupt the ability of GFP to form anti-parallel dimers (Zacharias et al., 2002), and examined the ability of the resulting fusion protein variant, LAMP1-mGFP, to elicit aggregation of late endocytic compartments. Wild-type murine fibroblasts were transiently transfected with plasmids encoding LAMP1-GFP or LAMP1-mGFP, and the following day were fixed, permeabilized and subsequently stained for endogenous Lamp1 using Cy3-conjugated secondary antibody. Images of GFP and Cy3 fluorescence were obtained for each of 117 and 134 randomly selected cells expressing LAMP1-GFP and LAMP1-mGFP, respectively, and saved using coded file names. On the basis of GFP fluorescence intensity, we estimated that the expression levels of the two fusion proteins

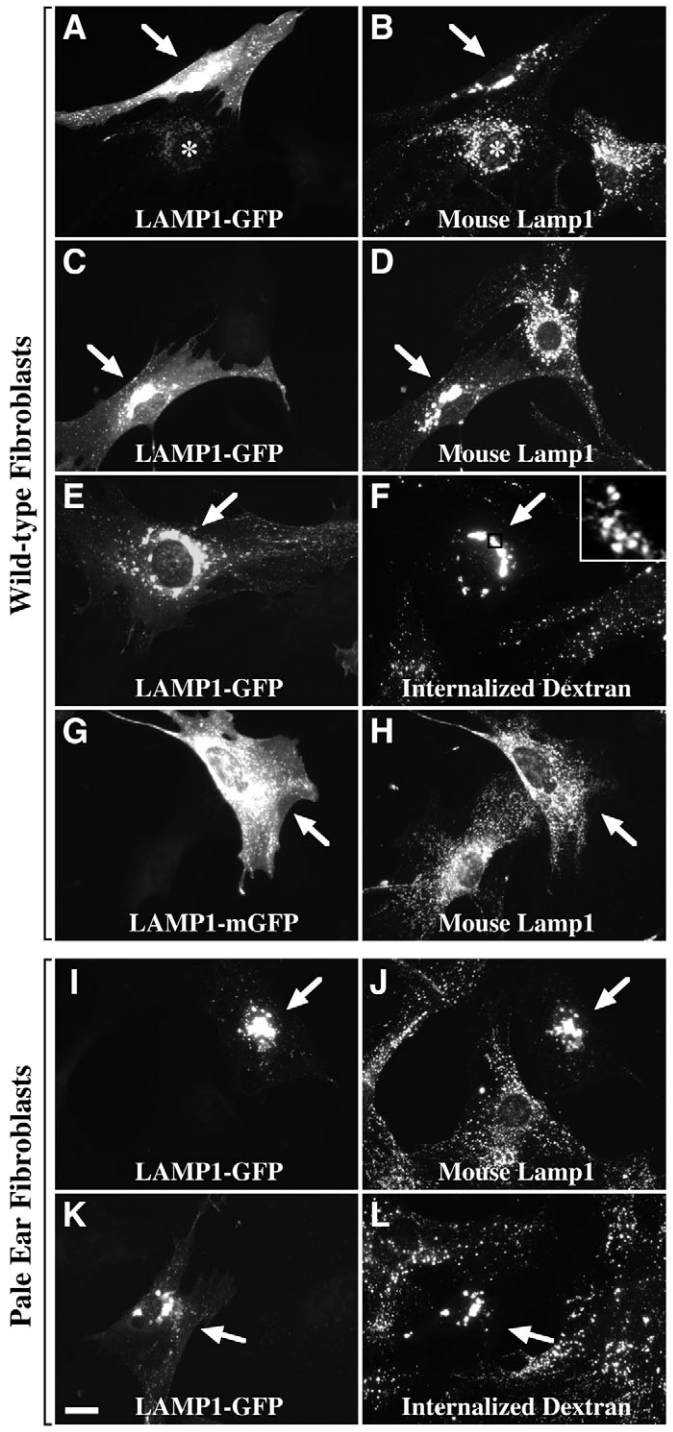


**Fig. 3.** High levels of LAMP1-GFP overexpression elicit aggregation of late endocytic compartments. Immortalized skin fibroblasts from wild-type (A-H) and pale ear (I-L) mice were transfected with plasmids encoding LAMP1 fused to either GFP or its non-dimerizing mutant form (mGFP). One day after transfection, cells were fixed/permeabilized and stained with the 1D4B antibody to mouse Lamp1 (B,D,H,J). In some experiments, cells were first allowed to internalize Texas-Red-conjugated dextran (F,L), transfected with the LAMP1-GFP-encoding plasmid, cultured for one day in medium without dextran, and then fixed and processed for fluorescence microscopy. Arrows indicate cells expressing high levels of LAMP1-GFP or LAMP-mGFP, as judged by their GFP fluorescence signal (A,C,E,G,I,K). Asterisks in A and B denote a transfected cell expressing LAMP1-GFP levels comparable with those of the cells shown in Fig. 2. Bar, 20 μm. The inset in F shows a high-resolution view of one of the dextran clusters as obtained by confocal microscopy, suggesting that the dextran-positive compartments have aggregated but not fused with each other.

were comparable; in arbitrary units, the median values were 33 and 41, and the ranges were 9-144 and 20-189, for cells expressing LAMP1-GFP and LAMP1-mGFP, respectively. The Cy3 fluorescence images, corresponding to endogenous Lamp1 staining, were scored by two observers who were not aware of the identity of the expressed construct or its expression level. Whereas 16 of the 117 LAMP1-GFP-expressing cells (14%) and 9 of the 11 cells expressing the highest LAMP1-GFP levels (82%) were scored as having 'chunky' Lamp1 staining by the two observers, none of the 134 cells expressing LAMP1-mGFP displayed such phenotype (e.g. see Fig. 3G,H). Therefore, the abnormal aggregation of lysosomes and late endosomes caused by LAMP1-GFP overexpression requires the ability of GFP to form dimers.

### Dynamics of late endocytic organelles in wild-type and mutant fibroblasts

Time-lapse fluorescence microscopy experiments were performed to test whether BLOC-3 is required for optimal movement of late endocytic compartments. A first set of experiments was carried out using wild-type and pale ear fibroblasts (three independent cell lines per strain) expressing low LAMP1-GFP levels comparable with those of the cells shown in Fig. 2. Subsequent experiments were carried out using cells expressing the non-dimerizing LAMP1-mGFP variant (two independent cell lines per strain) as well as cells in which lysosomes were specifically labeled using BODIPY-FL-conjugated dextran (one cell line per strain). In each case, ten cells per fibroblast line were analyzed by acquiring 50 consecutive GFP fluorescence images at 2-second intervals.

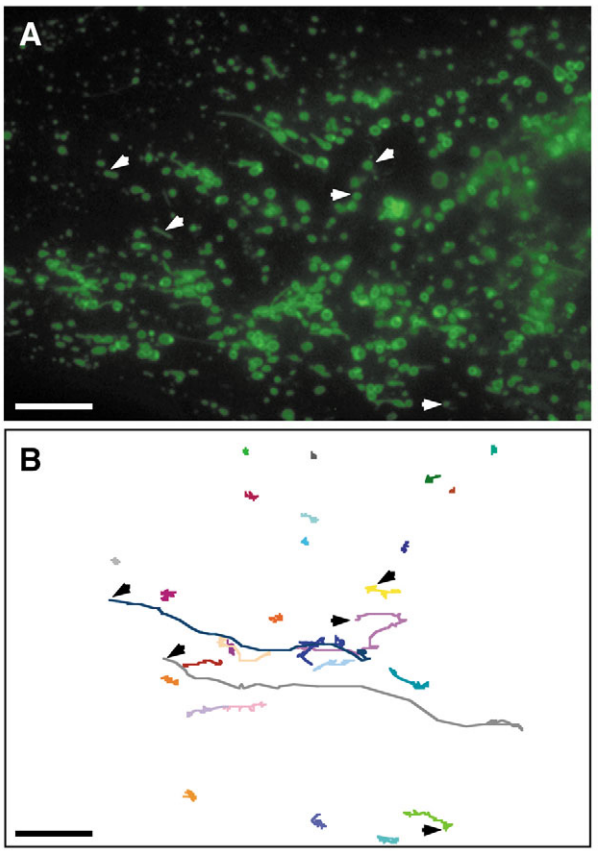


**Fig. 4.** Initial image (A) and examples of trajectories (B) observed in a representative time-lapse fluorescence microscopy experiment using wild-type murine fibroblasts expressing LAMP1-GFP. Arrowheads indicate the approximate initial positions of selected LAMP1-GFP-positive compartments that traveled significant effective distances during the course of the experiment. Bars, 20 μm.

Fig. 4A shows a portion of the initial image acquired from a wild-type cell expressing LAMP1-GFP. Consistent with previous studies on the dynamics of late endosomes and lysosomes (Matteoni and Kreiss, 1987; Cordonnier et al., 2001; Ko et al., 2001; Lebrand et al., 2002), the behavior of LAMP1-GFP-positive organelles was best described as a combination of short- and long-range movement events together with periods of no detectable movement, and the long-range movements required intact microtubules as judged by their dramatic inhibition in fibroblasts treated with nocodazole (not shown). Instances in which LAMP1-GFP-positive organelles adopted tubular shapes were observed (Fig. 4A and data not shown). Although one might envision that changes in shape could be a consequence of molecular motors pulling a large membrane-bounded organelle, we could not find any clear correlation between change of shape and organelle speed (not shown). By visual inspection of the time-lapse movies, it became apparent that lysosomes specifically labeled with BODIPY-FL-conjugated dextran were relatively less dynamic than LAMP1-GFP-positive organelles, suggesting that mature lysosomes might be less mobile than late endosomes or, alternatively, that loading of the lysosomal lumen with dextran might affect lysosome dynamics.

For quantitative analyses, we randomly selected 30 LAMP1-GFP-labeled organelles per cell, and for each organelle we determined its position at each frame. Examples of two-dimensional projections of the trajectories of selected LAMP1-GFP-positive organelles are depicted in Fig. 4B. For each organelle we calculated the maximum speed and effective distance, the latter defined as the largest distance between any two positions in the trajectory. Fig. 5 shows the distributions of maximum speed (panel A) and effective distance (panel B) corresponding to 900 LAMP1-GFP-positive organelles (30 organelles × 10 cells × 3 cell lines) from wild-type fibroblasts and the same number of organelles from pale ear (BLOC-3-deficient) fibroblasts. Panels A and B of Fig. 5 also show the corresponding distributions of LAMP1-GFP-positive organelles from wild-type cells treated with nocodazole, which allowed us to infer the extent of microtubule-dependent movement as assessed by our system. In particular, movement of LAMP1-GFP-positive organelles in nocodazole-treated wild-type cells only rarely achieved or exceeded an instant speed of 0.78 μm/second (corresponding under our imaging conditions to a displacement of 4 pixels between two consecutive frames; Fig. 5A) and never exceeded an effective distance of 4 μm (Fig. 5B). Interestingly, a relatively larger fraction of organelles from pale ear cells displayed maximum speed values of less than 0.78 μm/second (Fig. 5A) and traveled effective distances of less than 4 μm (Fig. 5B). Similar shifts in maximum speed and effective distance distributions were observed in experiments using wild-type and pale ear cells expressing the LAMP1-mGFP variant construct or labeled with BODIPY-FL-conjugated dextran (not shown).

To test whether the observed differences in maximum speed

and effective distance were statistically significant, for each variable we calculated the median of the values obtained for 30 organelles per cell. The resulting median values per cell, which we considered as independent measurements, corresponded to different cell lines and fluorescent labels (i.e. LAMP1-GFP, LAMP1-mGFP and BODIPY-FL-conjugated dextran) and were characterized by substantial variance (Fig. 5D,E and data not shown). Such variability might not only

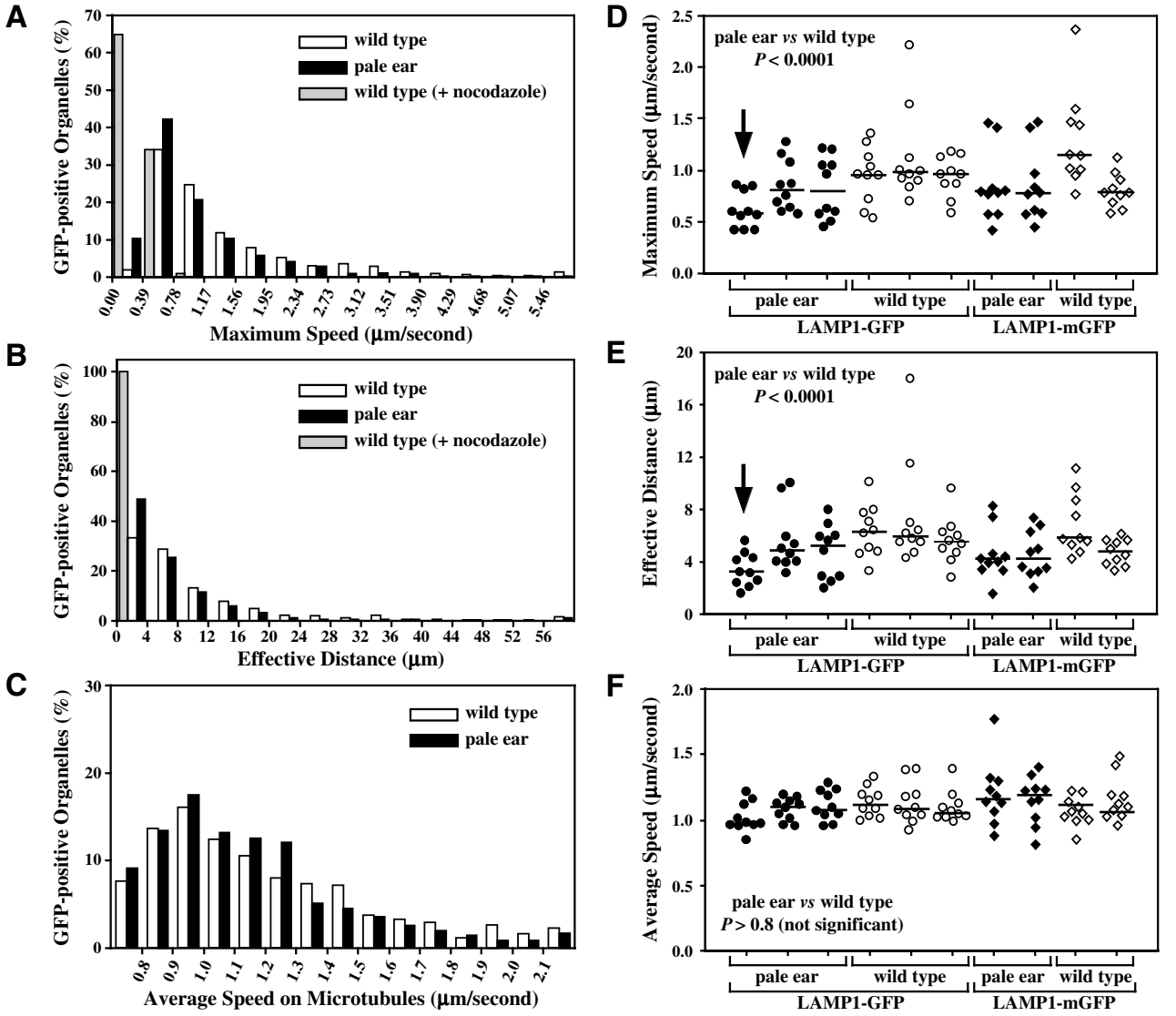


**Fig. 5.** Quantitative analyses of maximum speed (A,D), effective distance traveled during a 98-second period (B,E), and average speed of movements inferred to occur on microtubules based on instant speeds of at least 0.78 μm/second (C,F), obtained by time-lapse fluorescence microscopy analyses of LAMP1-GFP-positive organelles in fibroblasts derived from wild-type (open bars in A-C, open circles in D-F) and pale ear (black bars in A-C, filled circles in D-F) murine strains. Three independent fibroblast lines were analyzed per strain. For each fibroblast line, 10 cells expressing low LAMP1-GFP levels were examined by time-lapse fluorescence microscopy, and the movement of 30 randomly selected, LAMP1-GFP-positive organelles per cell was tracked and analyzed quantitatively. (A-C) Aggregate distributions of values obtained for 900 LAMP1-GFP-positive organelles (30 organelles × 10 cells × 3 fibroblast lines) per strain. Numbers on the x-axis denote bin limits; the last bin on the right includes all values greater than the upper limit of the previous bin, and the first bin on the left of C includes all values smaller than 0.8 μm/second. For comparison, the distributions are also included of maximum speed (A) and effective distance (B) of 120 LAMP1-GFP positive organelles (30 organelles × 4 cells) from wild-type fibroblasts that had been treated with nocodazole to disrupt microtubules (gray bars). (D-F) Median values per cell were plotted as individual data points, where the position on the y-axis represents the median value per cell and the position on the x-axis is arbitrarily chosen to group the data of the 10 cells analyzed for each fibroblast line. Median values obtained for cells expressing the LAMP1-mGFP variant construct and corresponding to two independent fibroblast lines derived from wild-type (open diamonds) and pale ear (filled diamonds) strains are also represented. Horizontal lines represent median values per data group. Statistical analysis of the data represented in D-F was performed using an ANOVA model upon logarithmic transformation, as described under Materials and Methods. The indicated *P* values correspond to the significance of 'genotype' (i.e. pale ear versus wild-type) as an explanatory variable. Exclusion of the data group highlighted by arrows in D and E from the ANOVA analysis did not modify the conclusion that the differences between wild-type and pale ear cells were statistically significant.

reflect cell-to-cell differences but also sampling error due to the analysis of only 30 organelles per cell; nevertheless, we chose to analyze a large number of cells rather than more organelles from fewer cells. We noticed that the median values per cell of maximum speed and effective distance followed normal (Gaussian) distributions upon logarithmic transformation (data not shown), thus allowing statistical analysis using an ANOVA model. A good fit of the data was obtained using genotype (i.e. wild-type and pale ear) and fluorescent label (i.e. LAMP1-GFP, LAMP1-mGFP and BODIPY-FL-conjugated dextran) as the explanatory variables; the fit improved only modestly upon consideration of 'cell line' as an explanatory variable, implying that the first two variables were sufficient to explain most of the variation in the data. For both maximum speed and effective distance, the effect of BLOC-3 deficiency (i.e. genotype) was statistically significant ($P<0.0001$), and so was the use of BODIPY-FL-conjugated dextran as a label ($P<0.0001$) instead of either LAMP1-GFP or LAMP1-mGFP (differences between the two fluorescent LAMP1 constructs were statistically not significant). We noticed that the values obtained for one pale ear cell line expressing LAMP1-GFP (Fig. 5D,E, arrow) were lower than those obtained for the other two pale ear cell lines expressing the same construct; nevertheless, exclusion of the data obtained using this cell line from the ANOVA analysis did not modify the main conclusion that the effect of BLOC-3 deficiency was statistically significant ($P<0.001$ for both maximum speed and effective distance). Consequently, we concluded that the maximum speed and effective distance of late endocytic compartments were reduced, albeit not dramatically, in BLOC-3-deficient cells.

We next considered the possibility that the observed differences in the dynamics of late endosomes and lysosomes between normal and BLOC-3-deficient cells could reflect deficiencies in their movement on microtubules. To address this possibility, we took advantage of the observation that LAMP1-positive organelles almost never moved at 0.78 μm/second or faster in nocodazole-treated cells (Fig. 5A). We chose this speed value as a threshold with which to select movement events that most probably occurred on microtubules. For each of the LAMP1-GFP-positive and LAMP1-mGFP-positive organelles analyzed as described above, we calculated the fraction of time traveled at instant speeds matching or exceeding the 0.78 μm/second threshold (Fig. 6A), as well as the average speed of this subset of movement events (referred to as average speed on microtubules; Fig. 5C and data not shown). For statistical analyses, median values per cell were calculated as described above for the other variables. The median values per cell calculated for average speed on microtubules (Fig. 5F) followed normal distributions upon logarithmic transformation and, hence, could be analyzed using an ANOVA model. In this case, however, the effect of BLOC-3 deficiency was statistically not significant ($P>0.8$). By contrast, a relatively higher fraction of late endocytic compartments within pale ear cells moved less than 2% of the time at the threshold speed or faster, regardless of whether the compartments were labeled with LAMP1-GFP or LAMP1-mGFP variants (Fig. 6A). The data obtained for this variable could not be analyzed using an ANOVA model because a large fraction of the median values per cell were zero, thus making it impossible to achieve a

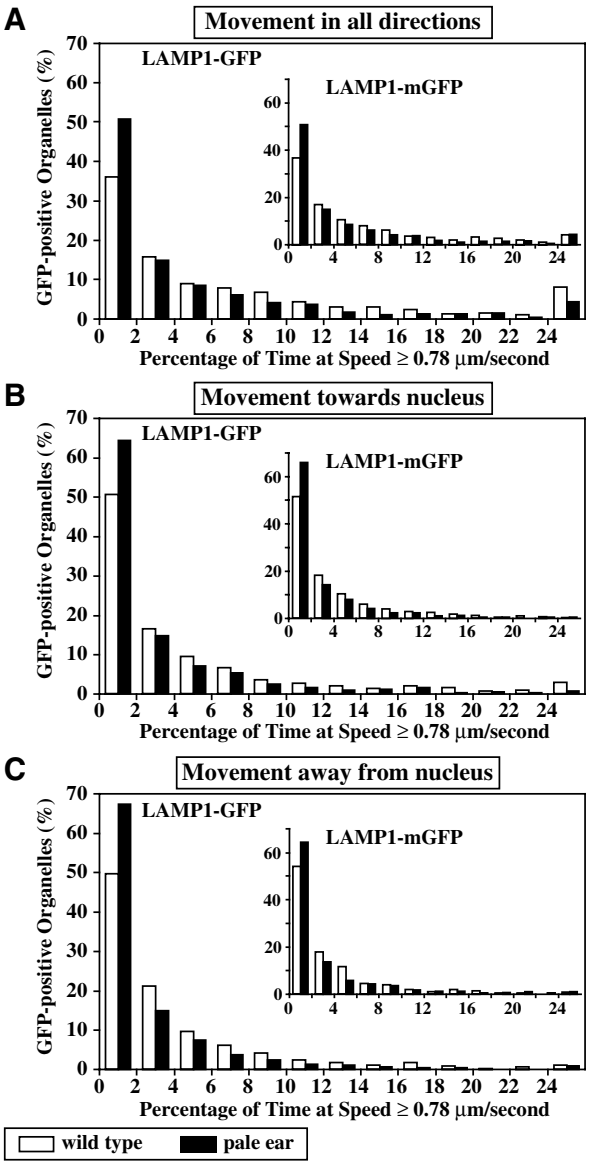


**Fig. 6.** Distributions of percentages of time in which 900 LAMP1-GFP-positive organelles within wild-type (open bars) or pale ear (closed bars) fibroblasts moved at instant speeds of 0.78 μm/second or faster, in any direction (A), towards the nucleus (B), or away from the nucleus (C). Insets, comparable distributions obtained for 600 organelles labeled with the LAMP1-mGFP variant construct expressed in wild-type (open bars) or pale ear (closed bars) fibroblasts. Numbers on the x-axis denote bin limits; the last bin on the right of each panel includes all values greater than 24%.

Gaussian distribution, even upon data transformation. For this reason, and because the most salient characteristic of the resulting distributions of median values per cell was the zero value, we applied Fisher's exact test to compare the relative odds of obtaining such value for wild-type and pale ear cells. To maximize statistical power, data obtained using cells expressing LAMP1-GFP or LAMP1-mGFP were pooled. The resulting pale ear/wild-type odds ratio was ~3.6, which was statistically significant ($P=0.0057$). Interestingly, similar differences were observed when organelle movement at instant

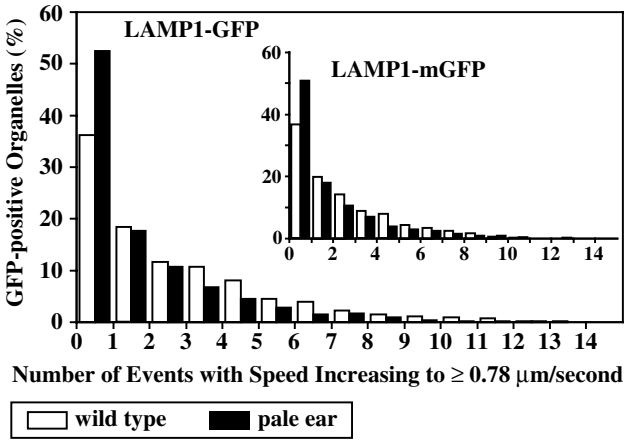


**Fig. 7.** Distributions of the number of events during a 98-second period in which the instant speed of each of 900 LAMP1-GFP-positive organelles within wild-type (open bars) or pale ear (closed bars) fibroblasts increased from less than 0.78 μm/second to reach or exceed this threshold speed. Insets, comparable distributions obtained for 600 organelles labeled with the LAMP1-mGFP variant construct within wild-type or pale ear cells. Numbers on the x-axis denote bin limits; the last bin on the right includes all values greater than 14.

speeds matching or exceeding the 0.78 μm/second threshold was analyzed taking into account its directionality, i.e. whether such movement was towards (Fig. 6B) or away from (Fig. 6C) the nucleus. Upon calculation of median values per cell, the odds of obtaining zero as a result were significantly higher among pale ear cells, both for movement towards the nucleus (odds ratio ~4.3, $P$=0.0016) and away from the nucleus (odds ratio ~3.7, $P$=0.0038). We also considered whether the observed differences in percentages of time traveling at the threshold speed or faster reflected a reduction in the number of events in which the organelle accelerated to match or exceed the threshold speed, and/or the duration of such events. The distribution of numbers of events with speed increasing to ⩾0.78 μm/second was shifted towards lower values in pale ear cells as compared with wild-type cells (Fig. 7), and the odds of obtaining zero as the median value per cell was significantly higher in pale ear cells (Fisher's exact test, $P$=0.005). By contrast, the distributions of the duration of such events revealed no statistical differences between wild-type and pale ear cells (not shown). Taken together, these results suggest that lack of BLOC-3 function negatively affects the ability of late endocytic organelles to attach productively to microtubule-dependent motors but does not influence significantly the duration or speed of these movement events.

## Discussion

In this paper, we describe the use of image analysis to estimate the degree of perinuclear accumulation of late endosomes and lysosomes in cells deficient in BLOC-1, -2 and -3. We also report time-lapse microscopy experiments in which the dynamics of Lamp1-positive organelles have been examined in wild-type and BLOC-3-deficient cells, and provide statistical evidence indicating that BLOC-3 function might regulate the ability of late endocytic organelles to attach productively to microtubule-dependent motors. Finally, we show that overexpression of LAMP1 fused to GFP at its cytoplasmic domain can elicit aggregation of late endocytic organelles by a mechanism that depends on the ability of GFP to form anti-parallel dimers.

Previous studies on the perinuclear clustering of organelles, including our own (Nazarian et al., 2003), have relied on the subjective judgement of an observer determining whether a given cell displays pronounced perinuclear accumulation or not, followed by comparison of different cell samples based on the percentages of cells determined to display such phenotype (e.g. see Matteoni and Kreiss, 1987; Poupon et al., 2003; Matsushita et al., 2004; Gissen et al., 2005; Hölttä-Vuori et al., 2005). Here, we have chosen to estimate the concentration gradient of the staining of an organelle marker around the perinuclear region as the PCI, thus allowing subsequent comparison of cell samples on the basis of their averaged PCI values. It should be emphasized, however, that the PCI is an approximation but not a real measure of such concentration gradient. A second limitation is that subjective judgment is still involved in delimiting the NP region areas necessary for calculation of the PCI. Nevertheless, the fact that the operator-to-operator variability was significantly lower than the cell-to-cell variability implies that such a subjective component should not have a major impact on the results. In any event, the images were analyzed following a 'blinded' approach in which the operator was unaware of the sample identity. Another limitation of the method described herein is that it is time-consuming. For these reasons, a fully automatic, image-processing method remains desirable. Finally, the method might not be sensitive enough to detect differences in perinuclear clustering of other organelle markers, or even of Lamp1 staining in cell types different from fibroblasts (e.g. cells that attach poorly to surfaces or with a high nucleus-to-cytoplasm ratio). Hence, its application to other systems may require optimization of experimental and image processing conditions.

Using the PCI approach, we have corroborated our previous observation that BLOC-3 deficiency results in decreased perinuclear clustering of Lamp1-positive, late endocytic organelles, and found no defects in perinuclear clustering of these organelles in mutant cells deficient in BLOC-1 or -2. As in the case of BLOC-3, BLOC-1 and -2 are expressed ubiquitously and mutations in the genes encoding at least some subunits cause HPS in humans and/or mice. However, their molecular function remains obscure (reviewed by Li et al., 2004; Di Pietro and Dell'Angelica, 2005). Fibroblasts derived from HPS patients bearing mutations in the gene encoding the HPS5 subunit of BLOC-2 have been shown to display exacerbated perinuclear clustering of late endocytic organelles containing LAMP3/CD63, with little or no staining observed in the vicinity of the plasma membrane (Huizing et al., 2004). By contrast, the same group reported that fibroblasts from patients carrying mutations in the gene encoding the HPS3 subunit of the same complex display normal distribution of LAMP3/CD63 staining (Gunay-Aygun et al., 2004). Although the PCI determined for three independent cell lines derived from cocoa mice (carrying mutations in the HPS3-encoding gene) seemed to be somewhat higher than the average PCI of wild-type cells (Fig. 1E), the differences were statistically not significant. In addition, we did not see any depletion of Lamp1

staining from the cell periphery of our cell samples. The reasons for the above discrepancies remain unclear.

To test whether BLOC-3 regulates the movement of late endosomes and lysosomes, we have performed time-lapse experiments using live cells expressing LAMP1 fused to either GFP or its non-dimerizing L221K variant, referred herein to as mGFP. At low expression levels, both fusion proteins were targeted correctly to late endocytic organelles, and no significant differences were observed in the dynamics of organelles labeled with LAMP1-GFP versus LAMP1-mGFP. Given the heterogeneity of organelles labeled with LAMP1-GFP or its variant, as well as the intrinsic variability between cells and between cell lines, large sets of time-lapse microscopic data were necessary to test for statistically meaningful differences between control and BLOC-3-deficient cells. For these analyses, we decided to consider each cell, rather than each tracked organelle, as an independent observation. We detected statistically significant differences between control and BLOC-3-deficient fibroblasts in the maximum speed and effective distance traveled by late endocytic organelles, even when the numeric differences were not too dramatic. Because these differences were suggestive of partial defects in organelle movement on microtubules, we defined the speed of 0.78 μm/second as a threshold with which to select those movement events that most probably occurred on microtubules. We realize that by using such a threshold value we may have filtered out movement events that were microtubule dependent but slow; such a limitation must be borne in mind during interpretation of the data. We attempted the alternative approach of performing time-lapse experiments using cells treated with actin-depolymerizing drugs (e.g. Latrunculin A) and assuming that all movement observed under these conditions would be microtubule dependent. However, the relatively large cells used in this study underwent significant changes of shape and partial detachment upon drug treatment, thus precluding acquisition of high-quality images (data not shown). Notwithstanding the potential limitations of using a threshold speed to study microtubule-dependent events, we were able to detect a relative decrease in the frequency of events in which labeled organelles within BLOC-3-deficient cells traveled at instant speeds equal or higher than the threshold. Interestingly, lack of BLOC-3 function affected movement on microtubules (i.e. at the threshold speed or higher) both towards and away from the perinuclear region, suggesting that productive attachment of late endocytic organelles to both dynein/dynactin and kinesins might be compromised. We considered the possibility that the observed differences could simply reflect the existence in BLOC-3-deficient cells of an extra pool of essentially immobile organelles, together with organelles with dynamics identical to those of control cells. However, upon exclusion of organelles that never moved at the threshold speed or faster from the data analysis, the resulting distributions still demonstrated a shift towards reduced frequencies of microtubule-dependent movement events for late endocytic organelles within BLOC-3-deficient cells (data not shown).

By which mechanism does BLOC-3 regulate late endocytic organelle movement? At least three scenarios can be considered. First, BLOC-3 could be directly involved in the attachment of these organelles to microtubule-dependent motors, although our results suggest that, if so, it should mediate attachment to both dynein and kinesin motors. The ability of a protein to regulate bidirectional, microtubule-dependent movement directly has previously been documented for dynactin and MEK/ERK bound to melanosomes (Deacon et al., 2003; Deacon et al., 2005), although not yet for proteins associated with late endosomes and lysosomes. Given that substantial movement of late endosomes and lysosomes was still observed in pale ear fibroblasts, one must conclude that BLOC-3 function is not essential for organelle attachment to microtubules. Hence, consideration of this first scenario would imply assuming that other cellular proteins can compensate in part for the lack of BLOC-3. Second, BLOC-3 function could be important for detaching late endocytic organelles from actin filaments. In such a scenario, lack of BLOC-3 function would increase the fraction of time spent by late endosomes and lysosomes on actin filaments, thus decreasing the fraction of time in which the organelles would be available for attachment to microtubules. This second scenario would provide a satisfactory explanation for the observations that BLOC-3 deficiency affected microtubule-dependent movement in both directions, and that the observed defects were partial. Third, BLOC-3 could play a rather indirect role, for instance by mediating the intracellular trafficking to late endosomes and lysosomes of a protein that, in turn, would be required for organelle attachment to microtubules and/or detachment from actin filaments. This third scenario, and not the first two, would be compatible with the intracellular localization reported for the HPS1 subunit of BLOC-3, which by immunogold labeling was found to be associated with tubulovesicular membrane profiles in the vicinity of the Golgi complex of lymphoblastoid cells (Oh et al., 2000). It is worth mentioning that a similar mechanism has been invoked to explain the defective movement of lytic granules, the lysosome-related organelles of cytotoxic T cells, in patients suffering from HPS-2 resulting from mutations in the gene encoding the β3A subunit of AP-3, a protein complex directly involved in protein trafficking (Clark et al., 2003).

How can the phenotype of BLOC-3-deficient fibroblasts be reconciled with the clinical manifestations of HPS-1 and -4? As mentioned in the introductory section, the main manifestations of these two forms of HPS are due to defects in cell-type-specific, lysosome-related organelles, namely melanosomes, platelet dense granules and lamellar bodies. Mild ceroid lipofuscinosis has also been described, at least for HPS-1, which could reflect modest defects in lysosomal function due to the observed abnormalities in organelle movement and localization. Conceivably, BLOC-3 could be required for normal movement and distribution of lysosome-related organelles and/or their precursors, and because melanosomes and platelet dense granules (and lamellar bodies?) co-exist with conventional lysosomes, one might even speculate that BLOC-3 could promote spatial segregation of maturing lysosomes and lysosome-related organelles to reduce the chances of heterotypic organelle fusion. Nevertheless, it is clear that future work will be necessary to establish the molecular function of BLOC-3 and its role in the pathogenesis of HPS.

During the course of this study, we noticed that high levels of LAMP1-GFP overexpression induced aberrant aggregation of late endocytic organelles, both in wild-type and BLOC-3-deficient cells. We observed that LAMP1-GFP overexpression

was capable of inducing aggregation of pre-existing lysosomes, as inferred from experiments involving loading of lysosomes with fluorescent dextran prior to transfection with the LAMP1-GFP-encoding plasmid (e.g. Fig. 3E,F). We also observed the aggregation phenomenon using different cell types and by overexpressing a construct consisting of human LAMP3/CD63 fused at its cytoplasmic domain to GFP (not shown). Because GFP is capable of low-affinity self-association, we considered the possibility that the observed aggregation of late endocytic organelles could be caused by low-affinity, anti-parallel dimerization of LAMP1-GFP molecules associated with the limiting membranes of opposing organelles. An analogous mechanism has recently been shown to mediate the formation of stacked ER membranes induced by overexpression of an ER-resident membrane protein tagged with GFP at its cytoplasmic domain (Snapp et al., 2003). In agreement with this idea, a point mutation introduced into the GFP domain of LAMP1-GFP to disrupt its ability to dimerize resulted in a variant fusion protein, LAMP1-mGFP, which failed to induce aggregation of late endocytic organelles at the highest expression levels achieved. Consequently, these results raise a note of caution on the interpretation of experiments in which aggregation of late endosomes and lysosomes is induced by overexpression of GFP-fusion proteins, and suggest that non-dimerizing mutant forms of GFP would be more appropriate tools for this type of experiments.

We thank M. J. Schibler at the Carol Moss Spivak Cell Imaging Facility for expert advice on time-lapse fluorescence microscopy, and S. M. Di Pietro for critical reading of the manuscript. This work was supported in part by National Institutes of Health grant EY015143.

## References

**Bakker, A. C., Webster, P., Jacob, W. A. and Andrews, N. W.** (1997). Homotypic fusion between aggregated lysosomes triggered by elevated $[Ca^{2+}]_i$ in fibroblasts. *J. Cell Sci.* **110**, 2227-2238.

**Bucci, C., Thomsen, P., Nicoziani, P., McCarthy, J. and van Deurs, B.** (2000). Rab7: a key to lysosome biogenesis. *Mol. Biol. Cell* **11**, 467-480.

**Burkhardt, J. K., Echeverri, C. J., Nilsson, T. and Vallee, R. B.** (1997). Overexpression of the dynamitin (p50) subunit of the dynactin complex disrupts dynein-dependent maintenance of membrane organelle distribution. *J. Cell Biol.* **139**, 469-484.

**Cantalupo, G., Alifano, P., Roberti, V., Bruni, C. B. and Bucci, C.** (2001). Rab-interacting lysosomal protein (RILP): the Rab7 effector required for transport to lysosomes. *EMBO J.* **20**, 683-693.

**Chiang, P.-W., Oiso, N., Gautam, R., Suzuki, T., Swank, R. T. and Spritz, R. A.** (2003). The Hermansky-Pudlak syndrome 1 (HPS1) and HPS4 proteins are components of two complexes, BLOC-3 and BLOC-4, involved in the biogenesis of lysosome-related organelles. *J. Biol. Chem.* **278**, 20332-20337.

**Clark, R. H., Stinchcombe, J. C., Day, A., Blott, E., Booth, S., Bossi, G., Hamblin, T., Davies, E. G. and Griffiths, G. M.** (2003). Adaptor protein 3-dependent microtubule-mediated movement of lytic granules to the immunological synapse. *Nat. Immunol.* **4**, 1111-1120.

**Cordonnier, M.-N., Dauzonne, D., Louvard, D. and Coudrier, E.** (2001). Actin filaments and myosin I alpha cooperate with microtubules for the movement of lysosomes. *Mol. Biol. Cell* **12**, 4013-4029.

**Deacon, S. W., Serpinskaya, A. S., Vaughan, P. S., Fanarraga, M. L., Vernos, I., Vaughan, K. T. and Gelfand, V. I.** (2003). Dynactin is required for bidirectional organelle transport. *J. Cell Biol.* **160**, 297-301.

**Deacon, S. W., Nascimento, A., Serpinskaya, A. S. and Gelfand, V. I.** (2005). Regulation of bidirectional melanosome transport by organelle bound MAP kinase. *Curr. Biol.* **15**, 459-463.

**Dell'Angelica, E. C., Ohno, H., Ooi, C. E., Rabinovich, E., Roche, K. W. and Bonifacino, J. S.** (1997). AP-3: an adaptor-like protein complex with ubiquitous expression. *EMBO J.* **16**, 917-928.

**Di Pietro, S. M., Falcón-Pérez, J. M. and Dell'Angelica, E. C.** (2004). Characterization of BLOC-2, a complex containing the Hermansky-Pudlak syndrome proteins HPS3, HPS5 and HPS6. *Traffic* **5**, 276-283.

**Di Pietro, S. M. and Dell'Angelica, E. C.** (2005). The cell biology of Hermansky-Pudlak syndrome: recent advances. *Traffic* **6**, 525-533.

**Gissen, P., Johnson, C. A., Gentle, D., Hurst, L., Doherty, A., O'Kane, C. J., Kelly, D. A. and Maher, E. R.** (2005). Comparative evolutionary analysis of VPS33 homologues: genetic and functional insights. *Hum. Mol. Genet.* **14**, 1261-1270.

**Gunay-Aygun, M., Huizing, M. and Gahl, W. A.** (2004). Molecular defects that affect platelet dense granules. *Semin. Thromb. Hemost.* **30**, 537-547.

**Harada, A., Takei, Y., Kanai, Y., Tanaka, Y., Nonaka, S. and Hirokawa, N.** (1998). Golgi vesiculation and lysosome dispersion in cells lacking cytoplasmic dynein. *J. Cell Biol.* **141**, 51-59.

**Hölttä-Vuori, M., Alpy, F., Tanhuanpää, K., Jokitalo, E., Mutka, A.-L. and Ikonen, E.** (2005). MLN64 is involved in actin-mediated dynamics of late endocytic organelles. *Mol. Biol. Cell* **16**, 3873-3886.

**Huizing, M., Hess, R., Dorward, H., Claassen, D. A., Helip-Wooley, A., Kleta, R., Kaiser-Kupfer, M. I., White, J. G. and Gahl, W. A.** (2004). Cellular, molecular and clinical characterization of patients with Hermansky-Pudlak syndrome type 5. *Traffic* **5**, 711-722.

**Jordens, I., Fernandez-Borja, M., Marsman, M., Dusseljee, S., Lansseen, L., Calafat, J., Janssen, H., Wubbolts, R. and Neefjes, J.** (2001). The Rab7 effector protein RILP controls lysosomal transport by inducing the recruitment of dynein-dynactin motors. *Curr. Biol.* **11**, 1680-1685.

**Ko, D. C., Gordon, M. D., Jin, J. Y. and Scott, M. P.** (2001). Dynamic movements of organelles containing Niemann-Pick C1 protein: NPC1 involvement in late endocytic events. *Mol. Biol. Cell* **12**, 601-614.

**Lebrand, C., Corti, M., Goodson, H., Cosson, P., Cavalli, V., Mayran, N., Fauré, J. and Gruenberg, J.** (2002). Late endosome motility depends on lipids via the small GTPase Rab7. *EMBO J.* **21**, 1289-1300.

**Li, W., Rusiniak, M. E., Chintala, S., Gautam, R., Novak, E. K. and Swank, R. T.** (2004). Murine Hermansky-Pudlak syndrome genes: regulators of lysosome-related organelles. *BioEssays* **26**, 616-628.

**Martina, J. A., Moriyama, K. and Bonifacino, J. S.** (2003). BLOC-3, a protein complex containing the Hermansky-Pudlak syndrome gene products HPS1 and HPS4. *J. Biol. Chem.* **278**, 29376-29384.

**Matsushita, M., Tanaka, S., Nakamura, N., Inoue, H. and Kanazawa, H.** (2004). A novel kinesin-like protein, KIFBβ3 is involved in the movement of lysosomes to the cell periphery in non-neuronal cells. *Traffic* **5**, 140-151.

**Matteoni, R. and Kreiss, T. E.** (1987). Translocation and clustering of endosomes and lysosomes depends on microtubules. *J. Cell Biol.* **105**, 1253-1265.

**Mu, F.-T., Callaghan, J. M., Steele-Mortimer, O., Stenmark, H., Parton, R. G., Campbell, P. L., McCluskey, J., Yeo, J.-P., Tock, E. P. C. and Toh, B.-H.** (1995). EEA1, an early endosome-associated protein. EEA1 is a conserved α-helical peripheral membrane protein flanked by cysteine 'fingers' and contains a calmodulin-binding IQ motif. *J. Biol. Chem.* **270**, 13503-13511.

**Nazarian, R., Falcón-Pérez, J. M. and Dell'Angelica, E. C.** (2003). Biogenesis of lysosome-related organelles complex 3 (BLOC-3): a complex containing the Hermansky-Pudlak syndrome (HPS) proteins HPS1 and HPS4. *Proc. Natl. Acad. Sci. USA* **100**, 8770-8775.

**Oh, J., Liu, Z.-X., Feng, G. H., Raposo, G. and Spritz, R. A.** (2000). The Hermansky-Pudlak syndrome (HPS) protein is part of a high molecular weight complex involved in biogenesis of early melanosomes. *Hum. Mol. Genet.* **9**, 375-385.

**Patki, V., Virbasius, J., Lane, W. S., Toh, B.-H., Shpetner, H. S. and Corvera, S.** (1997). Identification of an early endosomal protein regulated by phosphatidylinositol 3-kinase. *Proc. Natl. Acad. Sci. USA* **94**, 7326-7330.

**Patterson, G. H. and Lippincot-Schwartz, J.** (2002). A photoactivatable GFP for selective photolabeling of proteins and cells. *Science* **297**, 1873-1877.

**Poupon, V., Stewart, A., Gray, S. R., Piper, R. C. and Luzio, J. P.** (2003). The role of mVps18p in clustering, fusion, and intracellular localization of late endocytic organelles. *Mol. Biol. Cell* **14**, 4015-4027.

**Santama, N., Krijnse-Locker, J., Griffiths, G., Noda, Y., Hirokawa, N. and Dotti, C. G.** (1998). KIF2β, a new kinesin superfamily protein in non-neuronal cells, is associated with lysosomes and may be implicated in their centrifugal translocation. *EMBO J.* **17**, 5855-5867.

**Schroer, T. A.** (2000). Motors, clutches and brakes for membrane traffic: a commemorative review in honor of Thomas Kreiss. *Traffic* **1**, 3-10.

**Snapp, E. L., Hegde, R. S., Francolini, M., Lombardo, F., Colombo, S.,**

**Pedrazzini, E., Borgese, N. and Lippincott-Schwartz, J.** (2003). Formation of stacked ER cisternae by low affinity protein interactions. *J. Cell Biol.* **163**, 257-269.

**Taunton, J., Rowning, B. A., Coughlin, M. L., Wu, M., Moon, R. T., Mitchison, T. J. and Larabell, C. A.** (2000). Actin-dependent propulsion of endosomes and lysosomes by recruitment of N-WASP. *J. Cell Biol.* **148**, 519-530.

**Valetti, C., Wetzel, D. M., Schrader, M., Hasbani, M. J., Gill, S. R., Kreiss, T. E. and Schroer, T. A.** (1999). Role of dynactin in endocytic traffic: effects of dynamitin overexpression and colocalization with CLIP-170. *Mol. Biol. Cell* **10**, 4107-4120.

**Zacharias, D. A., Violin, J. D., Newton, A. C. and Tsien, R. Y.** (2002). Partitioning of lipid-modified monomeric GFPs into membrane microdomains of live cells. *Science* **296**, 913-916.